ОБЪЕДИНЕННЫЙ
ИНСТИТУТ
ЯДЕРНЫХ
ИССЛЕДОВАНИЙ

Дубна

E13-2000-243

A.G.Artukh, A.G.Semchenkov[1], G.F.Gridnev,
M.Gruszecki[2], F.Koscielniak[2], O.V.Semchenkova[1],
Yu.M.Sereda[1], V.A.Shchepunov, J.Szmider[2],
Yu.G.Teterev, Yu.P.Severgin[3], B.V.Rozhdestvensky[2],
Yu.A.Myasnikov[3], N.F.Shilkin[3], E.A.Lamzin[3],
M.G.Nagaenko[3], S.E.Sytchevsky[3], I.N.Vishnevsky[1]

WIDE APERTURE MULTIPOLE MAGNETS OF SEPARATOR **COMBAS**

Submitted to «Nuclear Instruments and Methods A»

[1]SC «Institute for Nuclear Research» NAS of Ukraine, Ukraine;
E-mail: semchenkov@main1.jinr.ru
[2]Henryk Niewodniczanski Institute of Nuclear Physics, Krakow, Poland
[3]Efremov Research Institute of Electrophysical Apparatus,
St.-Petersburg, Russia

2000

1 Introduction

At present, two basic methods are used for production of radioactive ion beams in nuclear physics laboratories. With the first method, radioactive beams are produced in reactions of projectile fragmentation in a target at intermediate and high energies. The target is followed by a fragment separator, where the ions are separated according to their magnetic rigidities and momentum losses in a degrader, a thin foil placed at the intermediate focus of the separator. This method has the advantage of in-flight separation of fragments of any kind: very short-lived nuclei can be investigated immediately after their synthesis. The main problems of the fragment-separation technique are the contamination of secondary beams and, quite often, their rather low intensity. With the second technique, much more sophisticated, radioactive ions are produced in a target-ion source where the primary beam is stopped totally. The nuclear species produced in the target are extracted and pass through several stages of separation and acceleration. Multi-stage separation combined with preacceleration between the stages allows one to achieve a very high level of purification for a wide variety of radioactive ions. Some of the most short-lived species, however, cannot be produced by this technique.

Concerning the method of in-flight separation, an analysing system consists of three main parts: two magnet sections containing bending magnets and an energy degrader situated between the sections. The ions produced in nuclear reactions are analysed in the first section according to the P/Q ratio where P is the ion momentum and Q the ion charge state. Then, the ions pass through the degrader, which reduces their energy. The energy loss depends on atomic number Z and mass number A of isotopes. Finally, the second section provides achromatic focusing at the exit of the separator, i.e. the radial focus position depends on relative deviations of the atomic number Z, mass number A, and ion charge state Q (but not the momentum) from those of a separated ion.

The kinematic separator COMBAS has been built for experiments with heavy ion beams of intermediate energies accelerated in the cyclotron U-400M at the FLNR JINR (Figure 1). Apart from the main use as a separator, it can also work in a spectrometric mode. At the design stage, the main requirements to the separator were as follows: the possibility of working at magnetic rigidities of up to $4.5T \cdot m$, maximum possible angular and momentum acceptances, a high energy resolution at the intermediate focus, a maximum size of the production target (up to 5 mm), a quite short total length of the channel that should match with the available experimental area in the U-400M hall and minimization of the power consumption.

To meet the above requirements, the following ideas were implemented in the

Fig.1. Separator COMBAS in the cyclotron U-400M hall (FLNR JINR).

separator design:
1. The use of only wide aperture bending magnets, without aperture reducing quadrupoles, let us increase such important parameters as the momentum and angular acceptances. As a result, combined function magnets has to be used, i.e., magnets containing both bending dipole and focusing quadrupole field componens.
2. The same idea was used for multipole corrections: the second and third order multipole field components were introduced to the main (bending and focusing) field of the magnets. Besides, special adjusting magnets were designed as wide aperture dipoles containing higher order field components (hence, the separator has no special hexapole and octupole lenses reducing the aperture).
3. A large pole width of main magnets M_1, M_2 provided the required energy resolving power at the intermediate focus (for a given production target size).
4. The necessarily short total length of the channel was automatically provided by the requirements of high energy resolution and large acceptance of the separator.
5. Low energy dispersion at the intermediate focus let us keep the radial beam size relatively small for the required energy acceptance.
6. The mirror symmetry of the magnetic structure and the use of the multipole magnets considerably facilitated optimisation of ion optics, reduced the price of the project, and simplified the tuning and operation procedures of the apparatus.

The main optical parameters of the separator are listed in Table 1. The device is intended for separating particles in the range of magnetic rigidities from 0.5 to $4.5T$·m within a solid angle of $6.4msr$ and energy acceptance of 40%. The degrader

Table 1
Main parameters of the separator COMBAS.

B_ρ	$T \cdot m$	4.5
Solid angle (maximum)	msr	6.4
Momentum acceptance (maximum)	%	20
Momentum resolution. Main object slit width $= 1mm$.	FWHM	4360
Momentum dispersion in the linear approximation		
at dispersion focus Fd normal to the optical axis	$cm/1\%$	1.53
Length of the channel	m	14.5

is used to separate isotopes by Z and A. It is wedge shaped to preserve the achromaticity at the final focus. The identification of separated particles can be performed by the TOF and dE-E methods. Short-lived exotic nuclei having lifetime as small as $1\mu s$ can be separated with the device.

The separator COMBAS has been commissioned and is used, at present, in experiments to study the mechanisms of nuclear reactions with heavy ions beams of N, O, S, Ne, Ar, and Ca at energies of $20 - 60MeV/A$.

2 Magnet structure of the separator COMBAS

The kinematic separator COMBAS (see Figure 2) is a complicated magnet channel with advanced ion-optical characteristics hitting the record in a class of similar experimental devices. Its structure and subsystems were described in detail in (1),(2). It has the following magneto-optical structure: $F_o M_1 M_2 M_3 M_4 F_d M_5 M_6 M_7 M_8 F_a$, where F_o is the production target, $M_1 - M_8$ are the magnets, F_d is the intermediate dispersive focus, and F_a is the exit achromatic focus. A short description of all the separator magnets is given in (3). The first two magnets, M_1 and M_2, are analysing ones, while the next two, M_3 and M_4, are a steering pair. The deflection angle is 25^o for each analysing magnet and 7.5^o for the steering magnets. The field direction of magnet M_4 is opposite to that of M_1-M_3. Due to this fact, the pair of the M_3 and M_4 magnets does not practically influence the 1^{st} order resolving power and the other 1^{st} order optical parameters. At the same time, the pair of magnets $M_3 - M_4$ performs both beam steering and corrections of the 2^{nd} and 3^{rd} order aberrations. A momentum slit placed at F_d separates ions according to their magnetic rigidities. In the F_d plane, a degrader is installed, in which ions lose their energy depending on their masses and nuclear charges.

The second section of the separator is a mirror symmetric with respect to the first one, the plane of symmetry being normal to the beam direction at F_d. It consists

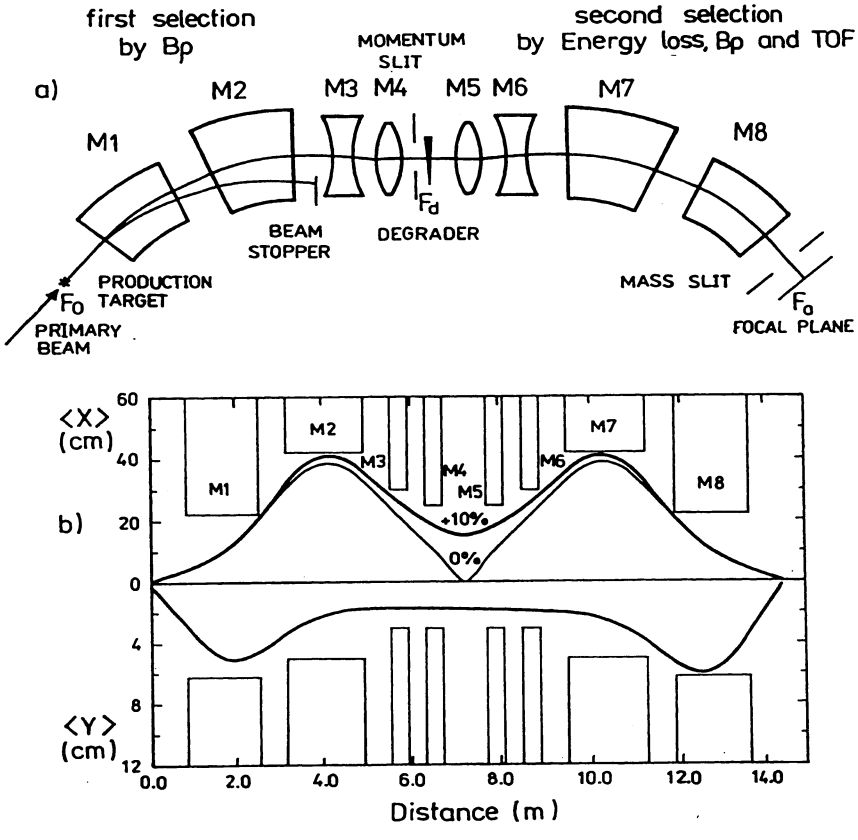

Fig.2. (a) Magneto-optical sketch of the separator COMBAS;
(b) Horizontal OX and vertical OY beam envelopes of the magnetic channel. The solid thick line is the contour of the $\delta = 10\%$ momentum acceptance; the thin line corresponds to $\delta = 0\%$.

of two pairs of magnets, M_5, M_6 (counterparts of M_4, M_3, respectively) and M_7, M_8 (counterparts of M_2, M_1). The second section of the separator compensates the momentum dispersion produced by the first section and collects fragments at the exit achromatic focus F_a. Horizontal positions of ions depend on deviations of fragment masses, nuclear charges, and ion charge states from those of the central fragment to be separated. The exit slit is located at F_a and provides final separation of the desired fragments from other species.

3 Optimization of optical parameters

The 1st order optical parameters of the separator have been optimised with the code BETRAMF (4). The high angular and momentum acceptances in combination with a high momentum resolution at the intermediate focus required to optimise the system with taking account of the non-linear distortions of the beam. The method of aberrational decomposition, widely used for designing broad range magnet spectrographs, was employed for calculating and optimising the COMBAS beam optics. The computer program TOREX (5), (6), calculating aberrational coefficients up to the 3^{rd} order by raytracing, was used for the calculations. The following form of aberrational decomposition is used in the program:

$$x^i = \sum_{q=1}^{\infty} \sum_{k_1 \ldots k_6 \geq 0}^{k_i + \ldots + k_6 = q} (x|x_1^{k_1} \ldots x_6^{k_6}) x_1^{k_1}(0) \ldots x_6^{k_6}(0) \qquad (1)$$

where $X = (x_1 \ldots x_6) = (x, p_x, y, p_y, \sigma, \delta)^T$ is the vector of a position of a particle in the phase space; x, y, and σ are the radial, vertical, and longitudinal deviations from the equilibrium particle; p_x, p_y and δ are the respective canonical momenta. In the linear approximation, p_x, p_y are equal to the angular deviations of a particle from the axis trajectory in the radial and vertical directions, and δ is equal to the relative deviation of the particle relativistic momentum from the particle momentum on the optical axis.

The system was optimised for an object (target) generating particles with coordinates uniformly distributed within the volume:

$$x^2 + y^2 \leq r^2, r = 2.5mm, \qquad p_x^2 + p_y^2 \leq p^2, p = 0.04rad, \qquad (2)$$

and with momentum deviations from -6% to $+6\%$. The aberrations at F_d were optimised so that the focal plane was normal to the beam direction, i.e. $(x|p_x\delta) = 0$. The most important 2^{nd} order aberrations deteriorating the momentum resolution were $(x|p_x^2)$, $(x|p_y^2)$, $(x|p_x\delta)$, $(x|xp_x)$, and $(x|x\delta)$. These aberrations together with the non-linear dispersion $(x|\delta^2)$ were minimized by introducing sextupole components in the field distributions in magnets $M_1 - M_4$ and by curving the effective field boundaries of M_3 and M_4. All the other 2^{nd} order aberrations were also taken into account in the minimization procedure to keep their values reasonably low. One should note the importance of the aberrations $(x|xp_x)$ and $(x|x\delta)$. This is due to rather big dimensions of the source (2) and wide momentum and angular angular acceptance. In the 3^{rd} order, the most important aberrations to be corrected were $(x|p_x^3)$, $(x|p^2\delta)$, $(x|p_x\delta^2)$, and $(x|p_xp_y^2)$. Octupole components introduced into the field distributions of magnets $M_1 - M_4$ minimized them.

Table 2
Designed quadrupole, sextupole, and octupole component parameters of the separator COMBAS magnets.

Magnets	R_{in}, cm	R_{out}, cm	n	β_2, cm^{-2}	β_3, cm^{-3}
$M_1(M_8)$	-	-	11.0024	0	$1.67 \cdot 10^{-8}$
$M_2(M_7)$	-	-	-6.75	$2.77 \cdot 10^{-7}$	$-4.02 \cdot 10^{-10}$
$M_3(M_6)$	-50	-50	0	$6.69 \cdot 10^{-7}$	$-2.38 \cdot 10^{-8}$
$M_4(M_5)$	50	50	0	$2.62 \cdot 10^{-6}$	$-1.46 \cdot 10^{-8}$

Monte Carlo trajectory simulations, performed after the optimisation, showed that the corrections considerably improved the momentum resolution at the focus F_d. Peaks with a momentum difference as small as 0.15% were resolved (at one-fourth of maximum) in the centre of the focal plane, while at both the borders of the momentum acceptance the resolution approached $0.2-0.3\%$. These results were considered acceptable.

Compensation for the aberrations at the achromatic focus F_a was done similarly, by introducing sextupole and octupole components in the field of magnets $M_5 - M_8$. The first order mirror symmetry of the device with respect to the intermediate focal plane facilitated that compensation, as some aberrations at F_a were zero due to the symmetry.

Apart from introducing sextupole and octupole components into the magnetic fields, special correcting coils were mounted on the pole pieces of magnets M_4 and M_5. These were assigned to correct small deviations (within a few per cent) of the field distribution from the design parameters.

4 Methods of introducing quadrupole, sextupole and octupole components into the magnets

As is known, higher order field components can be introduced into magnets in two ways: either by creating a radially variable field (by profiling the magnet pole pieces, shimming, and specially positioning the main magnet coils) or by profiling the entrance and exit pole faces. The first method was used to introduce quadrupole components into the fields of magnets $M_1(M_8)$ and $M_2(M_7)$, and sextupole and octupole components into the fields of all the magnets. The second method was applied to create extra sextupole components in steering magnets M_3, M_4 and M_5, M_6.

Table 2 presents field parameters of the magnets $M_1 - M_8$ found as a result of optimising the COMBAS optics up to the 3^{rd} order (see the previous section). In

the case of radial field variation, the field decomposition is defined by

$$B(\Delta R) = B_o(1 - n\frac{\Delta R}{R} + (\beta_2 R)\Delta R^2 + (\beta_3 R)\Delta R^3) \tag{3}$$

where $B_o = B(0)$ is the value of the field at the magnet center; n is the 1^{st} order field index; β_2 and β_3 are sextupole and octupole field components, respectively,

$$n = -\frac{R}{B_o}\partial B/\partial R, \beta_2 = \frac{1}{2!B_o R}\partial^2 B/\partial R^2, \beta_3 = \frac{1}{3!B_o R}\partial^3 B/\partial R^3, \tag{4}$$

The parameters n, β_2, and β_3 are proportional to the respective quadrupole, sextupole, and octupole strengths $S_1 - S_3$ (7): $S_1 = -nL/R^2$, $S_2 = \beta_2 L$, and $S_3 = \beta_3 L$, where L is the effective length. In the case of an entrance (exit) pole face curvature with the radius R_c, the respective sextupole strength S^2 is defined as $\frac{1}{2RR_c}$ (7). The quantity $R_{in}(R_{out})$ in Table 2 refers to the entrance (exit) radii of pole face curvatures in magnets $M_3 - M_6$.

To calculate the radial profiles of the pole pieces (in the central regions of magnets $M_1 - M_8$) which produce the required field distributions in the median planes, a special mathematical procedure was developed. The field scalar potentials defined in median planes were reconstructed in the volumes around median planes by the analytical continuation method. The pole profiles were calculated under the assumption that they are equipotential and that there is no saturation. The method was realized in the program POLUS (8) for the MCAD package. The obtained profiles were used as inputs for the program SCALAR (9) to recalculate them more precisely, with taking account of the saturation in the pole pieces. A 2D-aproximation was used in the program. This procedure was used only at the first stage of calculations. Large apertures and small effective lengths of the steering pairs of magnets M_3-M_4 and M_5-M_6 required the field analysis to be made with 3D-numerical simulations. The optimisation procedure was similar for all the magnets. A precision finite-element 3D-model of the magnet was developed and used for optimising the pole shape in the end regions of the magnets. This model allowed for the actual geometry of ferromagnetic and current coils. A consideration was made of the saturation effect (3). (Note that, for the steering pairs of magnets M_3-M_4 and M_5-M_6, the field varies drastically along the magnet length.) In addition, a comparison was made with the results of 2D-calculations with the SCALAR program and 3D-calculations with the KOMPOT (10) code for the central regions of all the magnets. The data obtained by different methods were found to be in good agreement.

5 Analysis of the effective lengths

Measured magnetic field distributions are very important to control the quality of real magnetic fields and, if necessary, to introduce corrections during the magnet manufacturing process. For example, on the basis of the measured field distributions in the median plane, the shimming of pole surfaces of magnets $M_3 - M_6$ (having rather complicated 3D-forms) was carried out. The 3D-measurements of magnetic field distributions (field maps) at different induction levels are very important for wide aperture magnets with non-uniform magnetic fields and they are necessary to simulate a realistic optical model of the separator. In particular, for a reliable ion identification with the TOF method, it is necessary to reconstruct the ion trajectory along the separator quite precisely. An optical model is also a skeleton for interpreting the measured beam parameters.

The experimental magnetic field distributions were analysed in different ways. The radial field variations were inspected to study how well they match the required radial field parameters (see Table 2). The longitudinal field behaviour was studied through calculating the effective lengths and via comparing these lengths with the design values obtained from the ion-optical optimisation of the entire system. The effective lengths were calculated from the magnetic field measurement data by using the effective length formula

$$L_{eff}(R+\Delta R) = \int B(R_o+\Delta R, X)dX/B(R_o+\Delta R, 0) \qquad (5)$$

where $B(R_o+\Delta R, X)$ is the vertical component of the magnetic field measured in the median plane in the radial and longitudinal coordinates $(R_o+\Delta R)$, and X, respectively.

The design lengths of sector magnets M_1, M_2, M_7, and M_8 are determined as

$$L(R_o+\Delta R) = (R_o+\Delta R)\varphi \qquad (6)$$

where R_o, ΔR, and φ are the bending radius of the central trajectory, the radial deviation from the central trajectory, and the magnet deflection angle, respectively. For the rectangular steering pairs of magnets $M_3(M_4)$ and $M_5(M_6)$ having entrance and exit pole face curvatures, the design lengths are defined as

$$L(R_o+\Delta R) = R_o \sin\varphi - 2R_c(1-\sqrt{(1-(\Delta R/R_c)^2)}) \qquad (7)$$

where R_c is the pole face curvature radius. The positive value of R_c corresponds to

the convex surface. One should note that the lengths were calculated for different radii, which allowed us also to study the radial variation of effective field boundaries at the entrance and exit of each magnet.

At the stage of the ion-optical optimisation of the separator it was found that an error of 0.2% in the effective field lengths is acceptable and would not cause a noticeable deterioration of the separator performances.

6 Basic characteristics of the magnets

The pair of multipole magnets M_1 and M_2 in the first analysing section of the separator (1), (2) determines the optical properties of the system in the linear approximation. Magnet M_1 focuses in the vertical plane and defocuses in the horizontal plane. The action of magnet M_2 is opposite. The 1^{st} order field indices of M_1 and M_2 are opposite in sign. Application of this magnetic structure allowed us, flexibly and efficiently, to form a beam of the required profile and size and, in addition, to facilitate minimization of the higher order spherical aberrations that considerably increase the image size in wide aperture systems.

Magnet M_1 (M_8) has a bending radius of $4m$, a deflection angle of 25^o, and a working magnetic path width of $\pm 200mm$ (see Figure 3). The gap between the pole pieces of magnets is varying, greater values of the gap correspond to greater bending radii. The pole pieces are of a special shape to produce quadrupole and octupole field components. The 1^{st} order field index equals 11.00, and the octupole component is also nonzero. The gap size is $120mm$ in the central ray region ($\Delta R = 0mm$); less than $50mm$, in the region of the minimum radius ($\Delta R = -200mm$); and more than $200mm$, for the maximum radius ($\Delta R = 200mm$).

Magnet M_2 (M_7) has a bending radius of $4m$, a deflection angle of 25^o, and a working magnetic path width of $400mm$ (see Figure 4). The vertical gap size varies with the radius in order to obtain the required fields components. The gap size is $100mm$ in the central ray region ($\Delta R = 0mm$); more than $300mm$, for the minimum radius ($\Delta R = -400mm$); and less than $50mm$, in the region of the maximum radius ($\Delta R = 400mm$). The 1^{st} order field index equals -6.75, and the sextupole and octupole field components are also nonzero.

Rather problematic was manufacturing of the shaped pole pieces of large size, which had to be magnetically identical. The four magnet poles of magnets M_1 and M_8 were manufactured from a single iron blank. A special rotary-table machine with the diameter of the rotating section of $10m$ was used to produce the pole pieces of identical shape and magnetic properties. The same procedure was employed to manufacture the pole pieces of magnets M_2 and M_7.

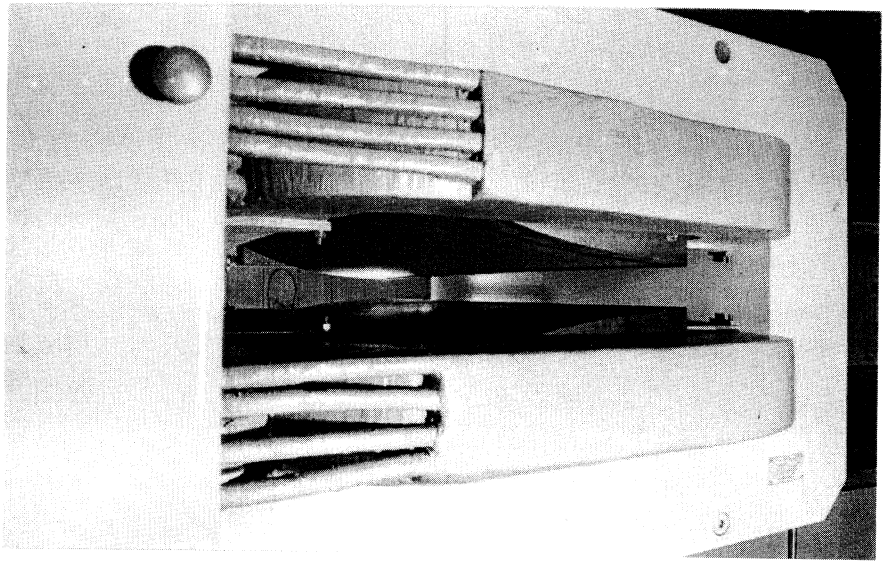

Fig.3. Analysing multipole magnet M_1.

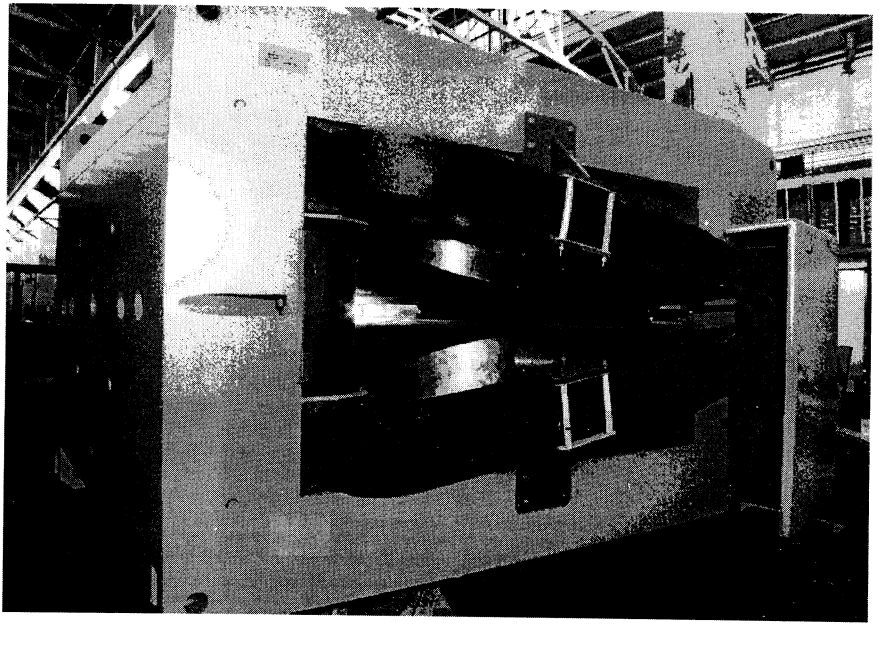

Fig.4. Analysing multipole magnet M_2.

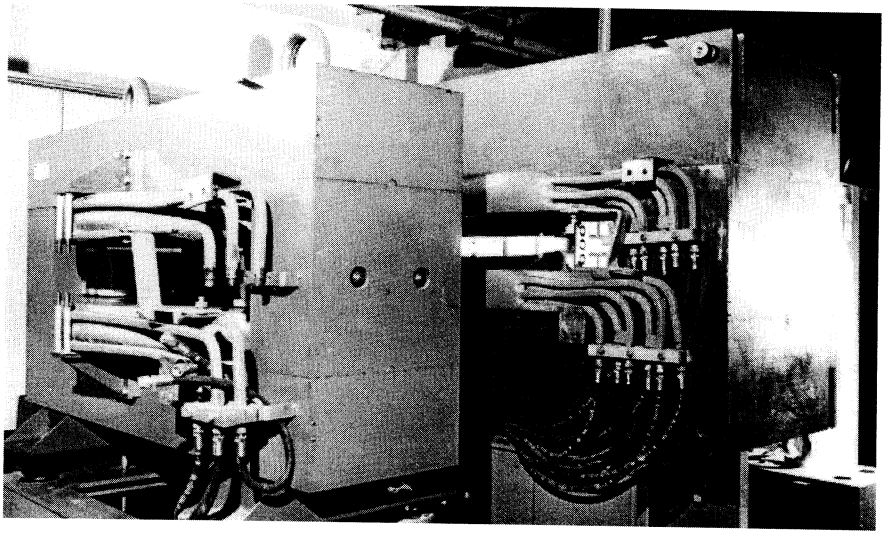

Fig.5. Steering multipole magnets M_4 (left) and M_3 (right).

Magnets $M_3(M_6)$ and $M_4(M_5)$ (see Figure 5) have $3m$ bending radii and 7.5^o deflection angles. The working magnetic path widths are $\pm 300mm$ for magnets M_3 (M_6) and $\pm 250mm$ for magnets $M_4(M_5)$. The gap sizes of magnets $M_3(M_6)$ and $M_4(M_5)$ on the central trajectory are equal to $60mm$. The vertical gaps vary with the bending radii to form the required higher order field components. In the 1^{st} order ions optics, the pairs of magnets M_3, M_4 and M_5, M_6 form parallel-to-parallel beam transfer systems with vertical focusing properties due to the fringe fields. Apart from the vertical focusing, the magnets correct the nonlinear beam distortions which could have been considerable, if not corrected, in such a wide aperture separating channel as COMBAS. Magnets $M_3 - M_6$ contain sextupole and octupole components in their field distributions to perform 2^{nd} and 3^{rd} order corrections of the aberrations at the intermediate and exit foci of the separator. Implementation of dipole magnets having specified higher order field components in their field distributions (instead of pure sextupole and octupole magnets) resulted in the considerable increase the momentum and angular acceptances of the separator.

The 3D-shapes of pole pieces of magnets $M_3 - M_6$ were calculated by the procedures described in section 5. To introduce addition sextupole components, the entrance and exit pole faces are curved with radii of curvature equal to $-50cm$ (concave effective field boundaries) in magnets $M_3(M_6)$ and $+50cm$ (convex effective field boundaries) in $M_4(M_5)$. All the magnets have zero quadrupole components. Magnets $M_3 - M_6$ are rectangular with collinear straight axes. (This substantially simplified the manufacturing process.) Due to small deflection angles and sufficiently large bending radii, the optical effect of sagitta is very small. The main technical

Table 3
Main parameters of magnets.

Parameters		Magnets $M_1(M_8)$	Magnets $M_2(M_7)$	Magnets $M_3(M_6)$	Magnets $M_4(M_5)$
Maximum induction on the central trajectory	T	1.125	1.125	1.5	1.5
Nominal induction on the central trajectory	T	0.875	0.875	1.167	1.167
Radius of the central trajectory	m	4	4	3	3
Working pole width	mm	400(±200)	800(±400)	600(±300)	500(±250)
Gap along the central trajectory	mm	120	100	60	60
Effective length	mm	1746	1746	393	393
Bending angle	deg	25	25	7.5	7.5
Resistance of main coils	Ω	0.07	0.07	0.03	0.034
Maximum current	A	950	960	900	900
Rated current	A	700	650	610	610
Maximum Voltage	V	70	68	30	20
Rated Voltage	V	50	48	20	13
Maximum Power	kW	66.5	65	27	13.5
Rated Power	kW	35	31.2	12	8
Inductance of main coils	H	0.17	0.3	0.08	0.04
Water discharge	$\frac{l}{min}$	23	28	22	9
Water overheating	^oC	40	40	18	30
Mass of copper	tns	1.1	1.0	0.5	0.33
Mass of steel	tns	13.3	25	6.6	2.3
Total magnet mass	tns	15	27	7.5	3

parameters of all the magnets are shown in Table 3.

7 Measuring and analysis of magnetic field distributions

7.1 Requirements to the accuracy of measurements

In the three-component magnetic field measurements, the Cartesian coordinate system was used with the origin $(0,0,0)$ at the centers of the magnets. The OX axis was tangential to the magnet optical axis at its center and followed the beam direction at this point. The OY radial axis positioned in the magnet central section was directed towards the greater bending radius. The OZ vertical axis was directed downward.

Magnetic measurements were organised so that the r.m.s. error $< \Delta B_z/B_{oz} >$ of measuring the main field component B_z at any mesh point inside the working volume of a magnet was not greater than $2 \cdot 10^{-3}$. With such an accuracy of a single measurement, the r.m.s. errors $< \Delta n_m >$ of determining the multipole field components (m - component number)

$$n_m = \frac{1}{m!} \frac{R_o^m}{B_{oz}} \frac{\partial^m B_z}{\partial y^m}, m = 1, 2, 3, \tag{8}$$

were less than the corresponding design tolerances (for chosen numbers of mesh points, see section 7.3) and were considered as acceptable for the purposes of field quality analysis and beam dynamics simulation studies. The values of $< \Delta n_m >$ are presented in Table 4.

The field measurement error due to the error of measuring the Hall probe voltage was less than $1G$. The main source of the B_z measurement errors was the error $< \Delta y >$ of positioning the Hall probe in the radial direction. Values of $< \Delta y >$ required to meet the established accuracy of $< \Delta B_z/B_{oz} >$ were found for each magnet from the relation

$$< \Delta y >= \frac{\Delta B_z}{|\partial B_z/\partial y|_{max}} \tag{9}$$

where the field derivatives are evaluated at the borders of magnetic paths of $M_2(M_7)$ and at the centers of $M_1(M_8)$. As one can see from Table 4, requirements to errors of the radial positioning were quite modest. The error $< \Delta z >$ in vertical positioning

Table 4
Errors of the calculation of multipole field components from measurement data at $< \Delta B_z/B_{zo} >= 2 \cdot 10^{-3}$ and required Hall probe positioning errors.

R. m. s. errors	Magnets $M_1(M_8)$	Magnets $M_2(M_7)$	Magnets $M_3(M_6)$	Magnets $M_4(M_5)$
$< \Delta n_1 >$	$0.74 \cdot 10^{-2}$	$0.53 \cdot 10^{-2}$	$0.89 \cdot 10^{-2}$	$1.10 \cdot 10^{-2}$
$< \Delta n_2 >$	0.049	0.027	0.044	0.066
$< \Delta n_3 >$	0.33	0.13	0.22	0.40
$< \Delta y >$ mm	0.7	1.0	0.6	0.4
$< \Delta z >$ mm	0.1	0.1	0.1	0.1
$< \Delta x >$ mm	1.0	1.0	1.0	1.0

of the probe, dedicated to measure radial component B_y, results in the error:

$$< \Delta B_y >= |\partial B_z/\partial y|_{max} \cdot < \Delta z >, \quad (\partial B_z/\partial y) = (\partial B_y/\partial z) \tag{10}$$

For the established error $< \Delta z >= 0.1mm$, the maximum values of $< \Delta B_y >$ were as large as $3.3G$, for the magnets M_2, M_7 and $4G$ for M_3, M_6, for example. As the values of B_y are relatively small near median planes, and derivatives $(\partial B_y/\partial z)$ are rather high, it was desirable to make the probe positioning error in the vertical direction as low as possible. Besides, in view of a small value of $< \Delta z >$, we could determine, with a high accuracy (less than $< \Delta z >$), the position of the median plane (where $B_y = 0$) for each measurement point in the plane (x, y) and investigate probable distortions of median planes in such big magnets as M_1, M_2, M_7, and M_8.

Field derivatives in the longitudinal OX direction are large only in the fringing field areas. The r.m.s. error $< \Delta x >$ of the longitudinal probe positioning was dictated by the required maximum error $< \Delta L_{EFB} >$ in determining of the position of the effective field boundary which had to be not greater than 1.0mm. The error $< \Delta x >$ = 1.0mm was sufficient to extract values of L_{EFB} from measurements with the required accuracy. In the course of field measurements, the accuracy of the head positioning was $0.1mm$ in all the three directions. As it follows from the above consideration, such positioning errors were sufficiently small and met all the above requirements.

The measurement of horizontal field components B_x and B_y made it absolutely necessary to determine the angles α_x and α_y of rotation of each probe in the measuring head (small rotations caused by assembling errors) around the two orthogonal axes OX and OY (with the accuracy $< \alpha >= 0.1^o$) and to take account of the Hall probe planar effect. All this required a special calibration procedure to be done for

Table 5
Parameters of the Hall probes used in the measuring head

Nominal Current	I	mA	100
Normal sensitivity	a	$\mu V/G$	11.1
Planar sensitivity	b	$\mu V/G^2$	$10.0 \cdot 10^{-6}$
Residual voltage	V_o	μV	6.0
Temperature coefficient		$\%/^oC$	-0.002
Size		mm^3	2.2 0.6

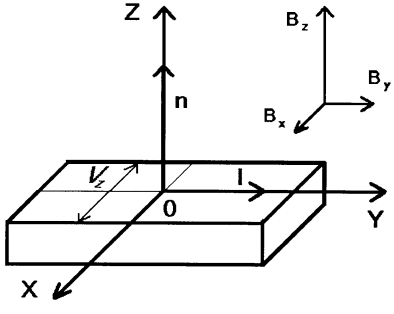

Fig.6. Orientation of a probe, dedicated for measurement of the B_z-component of the field (B_z-probe). The directions of the current I, of the Hall voltage V_z and of the normal n to the surface of the probe coincide respectively with axes OX, OY, and OZ of the local coordinate system connected with the probe.

the measuring head.

7.2 The calibration procedure of Hall probes

Technical parameters of the Hall probes used for magnet measurements are listed in Table 5. Note that the sensitivity of the Hall probe voltage to the temperature was $-0.002\%/C^o$, that is, too small to be taken into consideration in the measurements. (The variation of the temperature in the experimental area during measurements was not more than 5^oC.)

Figure 6 shows orientation of a B_z-probe dedicated for the measurement of the component B_z of the field. The normal n to the surface of the probe coincides with the direction of B_z; the direction of current I, with that of axis OY; and the Hall voltage V_z appears in the direction OX (index z shows that V_z gives the information about B_z). The Hall voltage V_z is connected with the components of vector B as

follows:

$$V_z(B) = V_{oz} + aB_z + bB_xB_y \tag{11}$$

where V_{oz} is the residual voltage, a and b are normal and planar field sensitivities, respectively (see Table 5).

Because of small angular errors in positioning of the Hall probe in the measuring head, it is sensitive not to the vector B but to a vector B' of the field in a new coordinate system (always strictly connected with a probe), whose orientation with respect to the original system is described by 3 angles α_x, α_y, and α_z (being, respectively, the angles of rotation around the axes OX, OY, and OZ, positive directions from OY to OZ, from OZ to OX, and from OX to OY). Components of the new vector B' depend on the components of B as follows:

$$\begin{aligned} B'_x &\cong B_x + \alpha_z B_y - \alpha_y B_z, \\ B'_y &\cong B_y + \alpha_x B_z - \alpha_z B_x, \\ B'_z &\cong B_z + \alpha_y B_x - \alpha_x B_y, \end{aligned} \tag{12}$$

So, the voltage of the B_z-probe can be rewritten as follows:

$$V_z(B) \cong V_{oz} + a(B_z + \alpha_y^{(z)} B_x - \alpha_x^{(z)} B_y) + bB_xB_y \tag{13}$$

where terms quadratic in the angles or those containing products $b\alpha_x$, $b\alpha_y$, $b\alpha_z$ were neglected, and upper indices (z) were attached to the angles to show that they refer to the B_z-probe. Figures 7a, 7b, and 7c show orientations of the 3 probes installed into the measuring head and dedicated for measuring the components B_z, B_x, and B_y, respectively. (Hereafter the field components are presented in a fixed coordinate system connected with a magnet, see Figure 7d.) Expressions for the Hall voltages V_x and V_y in B_x- and B_y-probes can be obtained from the expression for V_z through the substitutions: $B_z \rightarrow$-B_x and $B_x \rightarrow B_z$ for V_x and $B_y \rightarrow \quad B_x$, $B_z \rightarrow B_y$, $B_x \rightarrow B_z$ for V_y, which corresponding to rotations of the B_z-probe (in a fixed coordinate system of a magnet) transforming it into B_x- and B_y-probes:

$$V_x(B) \cong V_{ox} + a(-B_x + \alpha_y^{(x)} B_z - \alpha_x^{(x)} B_y) + bB_zB_y, \tag{14}$$

$$V_y(B) \cong V_{oy} + a(B_y + \alpha_y^{(y)} B_z - \alpha_x^{(y)} B_x) + bB_xB_z \tag{15}$$

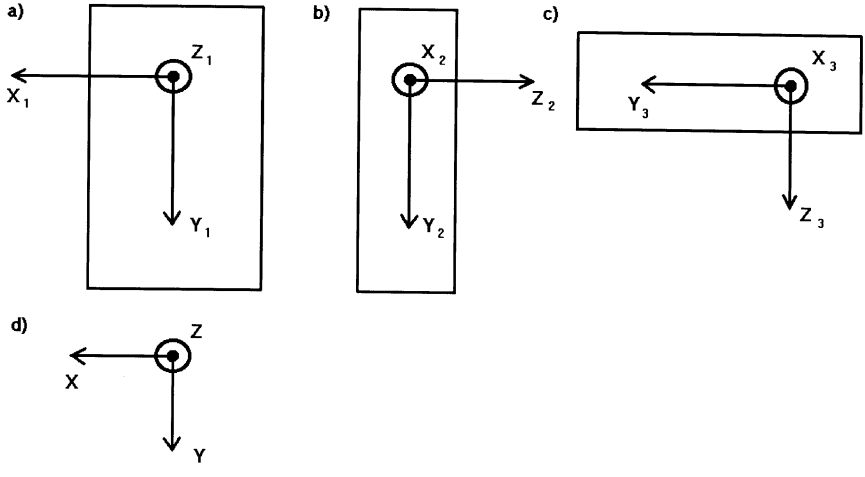

Fig.7. Orientations of the 3 mounted in the measuring head probes, B_z-probe (a), B_x-probe (b), and B_y-probe (c), with respect to the fixed coordinate system connected with a magnet (d). The axes of the 3 local coordinate systems strictly connected with the probes (as shown in Figure 6), are denoted by indices 1-3. If there are no orientation errors, the local coordinate system of the B_z-probe (a) coincides with the fixed coordinate system (d).

Note that, in the above expressions, angles $\alpha_{x,y}^{(x)}$ and $\alpha_{x,y}^{(y)}$ are defined in the local coordinate systems connected with the probes as it is shown in Figure 6. Upper indices (x) and (y) of angles show that they refer to B_x- and B_y-probes.

As one can understand from the expressions for V_x, V_y, and V_z, the contribution of the planar effect to the measured voltage V_z is negligible in the inside regions of magnets, where $B_y << B_z$ and $B_x << B_z$. On the contrary, voltages V_x and V_y are influenced by planar terms containing the product $b \cdot B_z$ which is approximately 1% of the Hall probe sensitivity a at $B_{oz} = 10,000G$. Hence, these planar terms had to be taken into account.

The Hall probe head was calibrated at the three field levels $B_o = 5,000$, $10,000$, and $15,000G$ at the center of a spectrometric magnet, where the field uniformity was very high. The value of the field B_o was controlled with an NMR magnetometer (of the measurement accuracy 0.001%). The purpose of calibration consisted in determining of the planar constant b, 6 angles $\alpha_{x,y}^{(x)}$, $\alpha_{x,y}^{(y)}$, and $\alpha_{x,y}^{(z)}$, as well as the normal Hall sensitivity a and residual voltages V_{ox},V_{oy}, and V_{oz}. To measure the planar constant b, the Hall voltage was measured for 36 positions of the probe corresponding to its rotation, with a step $\Delta\varphi = 10^o$ around the axis normal to its surface (axis OZ in Figure 6). The vector of the magnetic field was always in the probe plane (x, y) and rotated around axis OZ. The angular dependence of the

obtained Hall voltage $V(\varphi)$ was Fourier-analyzed to extract the amplitude of the 2^{nd} harmonic $\Delta V_2 = B_o^2 b/2$, used to calculate b (see Table 5). (The angular dependence $V(\varphi)$ comes from the planar term $bB_xB_y = bB_o^2 \cos\varphi \sin\varphi$ in the expression for V_z.)

The 6 angles $\alpha_{x,y}^{(x)}$, $\alpha_{x,y}^{(y)}$, and $\alpha_{x,y}^{(z)}$ were determined from measuring V_x , V_y , and V_z for 3 orientations of the head such that the field vector B contained only 1 nonzero component: $(B_o, 0, 0)$, $(0, B_o, 0)$, and $(0, 0, B_o)$. The measurements showed that absolute values of angles were within 1.8^o. The angular accuracy of the head positioning as well as the accuracy of determining the angles were 0.1^o.

7.3 Procedure of measurements

In the three-component field measurements of magnets M_1 (M_8) we used an automated magnetic measuring system (Figure 8) in the following composition:
1. Two heads for measuring the three components B_x, B_y, and B_z of the magnetic field. Each head was equipped with three Hall probes with size of $2 * 2 * 0.1mm$ spaced at intervals of $10mm$ along the axis OX. The accuracy of probe positioning within the measuring head was $0.1mm$.
2. Two monitoring probes to control the temperature and time stability during long magnetic measurements. The probes were placed in a narrow part of the gap with a high magnetic field of more than $10,000G$. The probes readouts were used to normalize the results of magnetic measurements.
3. A measuring carriage with an accuracy of $0.1mm$ equipped with two separable plates for the head installation.
4. Guides to move the measuring carriage inside the magnets. - An electrical drive with two step motors SHD-5 and a belt of stainless steel enabling the measuring carriage to be moved along the guides with an accuracy of $0.02mm$ (step of SHD-5) along the X- and Y-axes.
5. A channel for measuring the current of the Hall probes based on a SOLARTRON precision digital voltmeter (voltage measuring accuracy of $1\mu V$) with digital outputs and the SOLARTRON 7010 MINATE switch.
6. A computer control program for controlling the steppers, an eight-channel system for reading the measured data from the digital voltmeter and writing the data on an IBM PC hard disc according to the standard RS-232.

In the measuring plane, the heads moved automatically along the X- and Y-axis with a step of $20mm$. Along the Z-axis, the heads motion was hand-operated with a $10mm$ step. The measurements were made in 15 planes. The magnetic field was measured in a range of $1,280mm$ along the X-axis, $+200/-420mm$ along the Y-axis, and $70mm$ along the Z-axis (from the magnet centre) for three field levels at the centre: $B_o = 7,050G$, $B_o = 9,440G$, and $B_o = 11,600G$. The total number of measured points in each plane was more than 4,000.

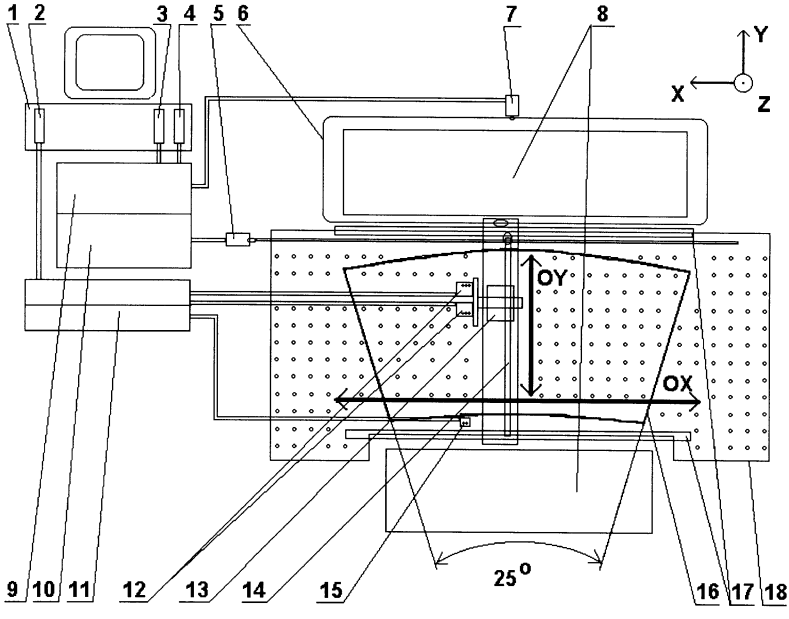

Fig.8. Block diagram of the automated system for measuring the magnetic field of magnets M_1 and M_8. The notation:
1- the control computer IBM PC;
2- the controller for connection with the SOLARTRON digital voltmeter;
3- the controller for the power supply assemblies of the X-coordinate displacement stepper;
4- the controller for the power supply assemblies of the Y-coordinate displacement stepper;
5- the Y-coordinate displacement stepper;
6- the X-coordinate displacement belt drive;
7- the X-coordinate displacement stepper;
8- the magnet M_1;
9- the power supply module for the X-coordinate displacement stepper;
10- the power supply module for the Y-coordinate displacement stepper;
11- the SOLARTRON precision digital voltmeter and the SOLARTRON 7010 MINATE switch;
12- two measuring heads, each having 3 Hall probes;
13- the measuring carriage;
14- the Y-coordinate displacement belt drive;
15- the monitoring Hall probes;
16- the area within effective field boundaries (deflection angle 25^o and radius $R_o = 4m$);
17- the measuring carriage guides;
18- the magnetic field measurement area.

The magnetization curve and the field distributions in the median plane of magnets M_2 and M_7 for three levels of the field $B_o = 7,300, 9,800, 11,600G$ were measured. The 3D- field distributions were also measured, for the same three field levels, on the surface of the closed volume between the pole pieces. A curvilinear coordinate system was used with the origin $(0,0,0)$ at the centres of the magnets. The $O\varphi$ axis was tangential to the magnet optical axis and followed the beam direction. The OY radial axis positioned in the magnet central section was directed towards a greater bending radius. The OZ vertical axis was directed downward.

The magnetic measurement procedure was as follows. First, the field was measured in the median plane. The measurement was carried out in two steps: in the region from the magnet entrance to the centre, and then from the magnet exit to the centre. The measured grid for each half of the median plane contained 42 points in the radial direction and 62 points in the beam direction. To match these two sets of measured data, common measured points at the centre of the magnet were used. The total number of the grid points, except for the repeated ones, was approximately 5,000. The fields in horizontal planes near the lower and upper pole pieces were measured similarly, with the total number of grid points of about 6,000 for every measurement along each pole piece. Then the field was measured in two vertical planes, for the minimum $(R_o - 200mm)$ and maximum $(R_o + 200mm)$ radii, at 2,000 and 1,000 points, respectively. Finally, measurements in the lateral planes (at the magnet entrance and exit) were made by using the carriage fixed with special pawls. More than 630 points were taken in each vertical plane. Thus, the total number of the measured points was more than 21,000 for each field.

The magnetization curve and field distributions in the median plane of magnets M_3 (M_6) and M_4 (M_5) for three levels of the magnetic field were measured $(B_o = 4,600G, B_o = 11,600G, B_o = 15,000G)$. The measuring head was always positioned in the magnet median plane with an accuracy of $0.1mm$. Along the OX and OY axes, the head was positioned with an accuracy of $0.2mm$. Before the measurements, the probes were calibrated at a special test bench in order to have a measurement accuracy of $2G$ (0.02% of the nominal magnetic field at the magnet centre). To reduce the measurement errors, the field was measured 5 times at each point. The r.m.s. error of field measurement due to the head positioning errors and the error of measuring the Hall probe voltage was estimated to be less than $3G$ (0.03% of the nominal field level). This corresponds to the required accuracy of field forming. The steps of measurements were: $dX = 20mm$ and $dY = 50mm$. The number of measured points was more than 700 for the magnets $M_3(M_6)$ and more than 550 for the $M_4(M_5)$.

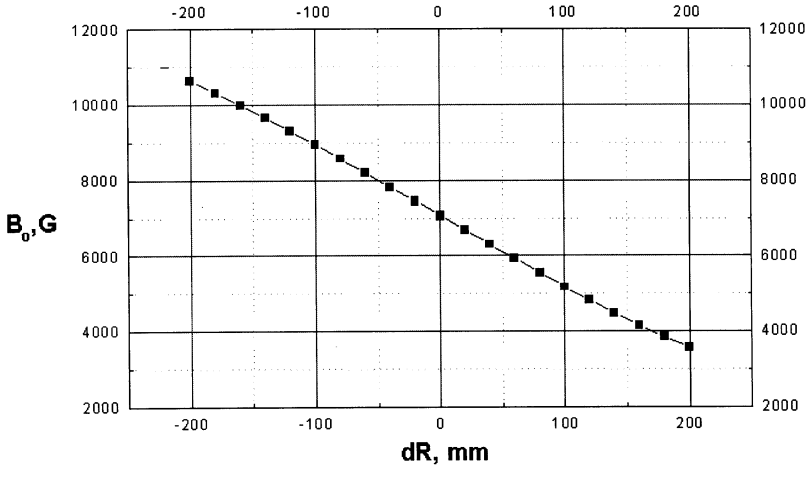

Fig.9. The magnetic field distribution in the central section of magnet M_1 at the field level $B_o = 7,050G$.

7.4 Analysis of the field distribution in the central section

The measurements showed that the difference between the field values in magnets M_1 and M_8 did not exceed 0.2%, and they were practically identical.

The magnetic field distribution in the central section of magnet M_1 is shown in Figure 9 for the field level $B_o = 7,050G$. Quadrupole and octupole components are observed in the distribution. The quadrupole component shows itself as a linear decrease of the field with increasing radii. (Respectively, the gap enlarges with increasing radii.) The octupole component contribution is seen in the slight deviation of the curve from the line at the minimum and maximum radii typical of 3rd order polynomials.

Analysis of the measured data showed that within the working magnetic paths of $\pm 200mm$ the deviation of the measured values from the calculated ones was not more than 0.1% for the field level $B_o = 7,050G$. This is a result of the good-quality magnet manufacturing. Some increase of errors in the minimum gap (or higher field) region at smaller radii is as large as 0.5%, which is probably due to the saturation effect. This can slightly decrease the working width of the magnet up to $\pm 150mm$ (75% of the nominal width) for magnetic rigidities of above $4.0T * m$.

The magnetic field distribution in the central section of magnet M_2 is shown in Figure 10 for the field level $B_o = 11,600G$. Quadrupole, sextupole, and octupole

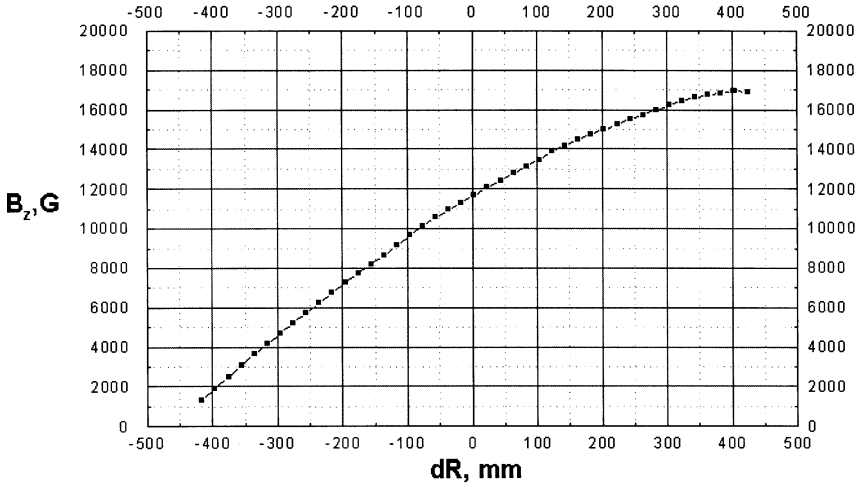

Fig.10. The magnetic field distribution in the central section of magnet M_2 at the field level $B_o = 11,600G$.

components are also observed in the distribution. The quadrupole component shows itself as a linear increase of the field with increasing radii. (Respectively, the gap decreases with increasing radii.) The sextupole and octupole components' contributions are seen as deviations of the curve from the line at the minimum and maximum radii.

Analysis of the measured data showed that the deviation of the measured values from the calculated ones was not more than 2.0% within the working magnetic paths of $\pm 400mm$, for all the three field levels $B_o = 7,200, 9,900$, and $11,600G$. In a smaller range of $\pm 350mm$, this error did not exceed 1% at the same field levels. A 2.0% error takes place in the region of larger radii (the smaller gaps and higher fields) where the saturation effect is noticeable. The saturation reduces the radial working width down to $\pm 350mm$ (about 90% of the nominal width) for magnetic rigidities higher than $4.0T \cdot m$.

The measured field maps revealed the identity of magnet pairs M_3, M_6 and M_4, M_5. For each pair, the difference between the field values at the same map points is less than 0.2%. On the other hand, the measured radial field variations are found to be different from those required by the design.

The measured radial field distributions at the centre of the median plane are shown in Figures 11 and 12 for magnets M_3 (M_6) and M_4 (M_5), respectively, for the field level $B_o = 4,600G$ in comparison with the required distributions.In magnets M_3, M_6, the sextupole and octupole components are strong and comparable. In the

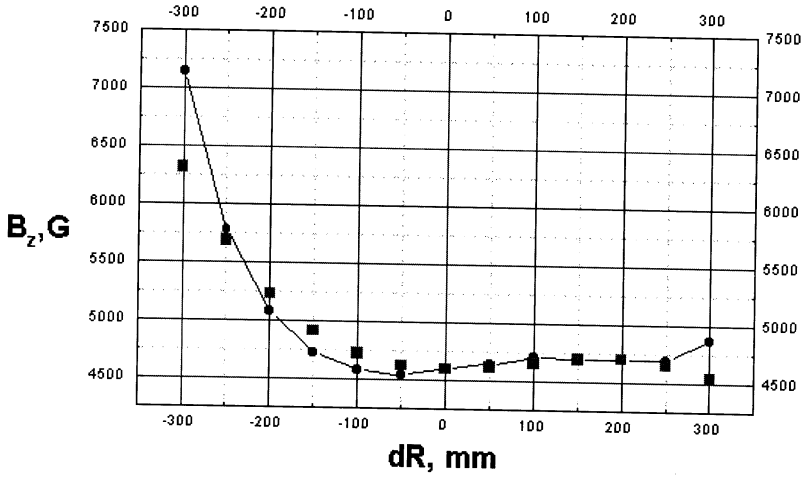

Fig.11. The magnetic field distribution in the central section of magnet M_3 at the field level $B_o = 4,600G$.

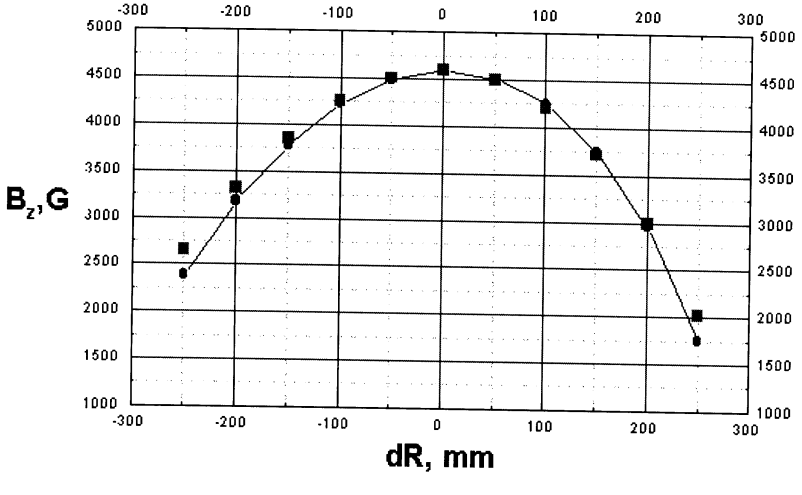

Fig.12. The magnetic field distribution in the central section of magnet M_4 at the field level $B_o = 4,600G$.

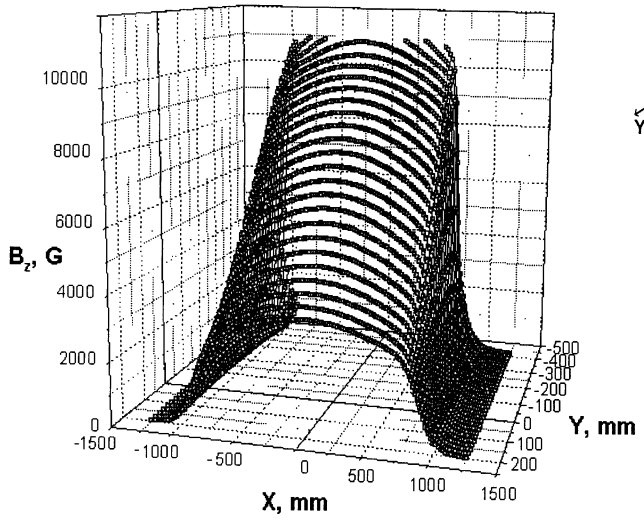

Fig.13. The measured distribution of the B_z-component of the magnetic field in the median plane of magnet M_1 at the field level $B_o = 7,050G$.

positive OY, they almost compensate for each other, resulting in a near-uniform field. The dominating field component in M_4, M_5 is a sextupole one (except for the dipole component). The asymmetry of the curve is slide, because the small octupole component is presents. The field deviations from the design values do not exceed 3% for M_3, M_6 and 2% for M_4, M_5. At the field levels $B_o = 11,600$ and $15,000G$ in magnets M_3 and M_6, they are less than 2.5% (for both the levels). For magnets M_4 and M_5, the deviation is 2.0% at $B_o = 11,600G$ and 1.5% at $B_o = 15,000G$.

7.5 Analysis of the field distribution in the median plane

From the point of view of nonlinear beam dynamics, the magnets of the separator are thin multipole lenses. To obtain the required optical performance of the magnets, it is necessary to provide the desired integral field distribution that can be tested through analysing the integral field distribution in the median plane. Analysis of the field in the median plane showed that both B_x (along the beam) and B_y (along the magnet axis) field components in the median plane are zero.

For magnet M_1, the B_z field component distribution along the OY axis is presented in Figure 13 for the field level $B_o = 11,600G$. The positive value of B_z corresponds to the direction downward. Analysis of the measured data showed that the effective length errors are less than 1.0%, 0.7% and 1.5% from the design value

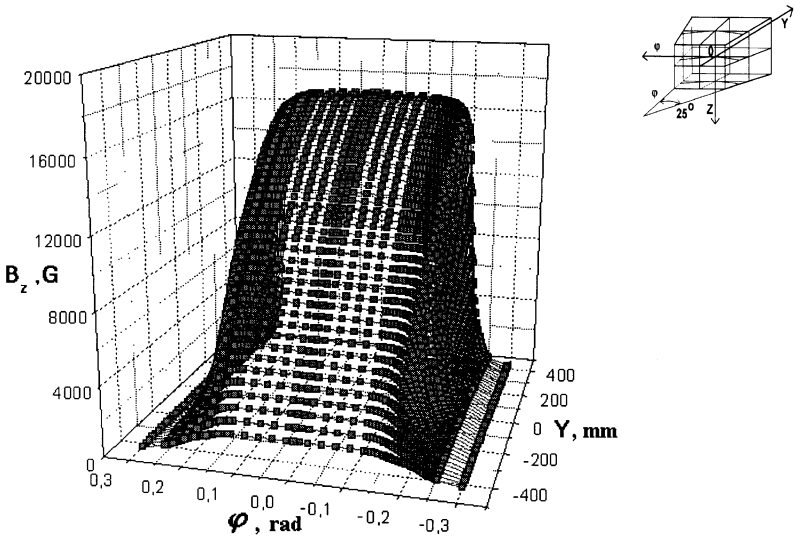

Fig.14. The measured distribution of the B_z-component of the magnetic field in the median plane of magnet M_2 at the field level $B_o = 11,600G$.

for the promising field levels $B_o = 7,050, 9,440$, and $11,600G$. The pole face rotation error in the fringing field areas is as large as 1.5^o, 1.0^o, and 0.5^o for the $B_o = 7,050, 9,440$, and $11,600G$, respectively.

The distribution of the B_z field component in the median plane of magnet M_2 is shown in Figure 14. Analysis of the measured data showed that the effective lengths of the both magnets exceed the design values at all the field levels $B_o = 7,200, 9,900$, and $11,600G$ and are slightly beyond the design tolerance (0.5%). This can be compensated by reducing the field values in a proper way to provide the nominal deflection angle of 25^o.

To analyse the effect of the deviations on the quality of the ion-optics characteristics at the intermediate and exit foci, an extra raytracing simulation was carried out with the use of the TOREX (6) and COSY INFINITY (11) codes. The simulation revealed, in particular, that beam trajectories cluster within the radial range of $\pm 200mm$ in magnets M_3, M_6 and $\pm 150mm$ in M_4, M_5. So the analysis and corrections were performed only within these working regions.

Figure 15 presents the measured field B_z in the median plane in magnet M_3 at the field level $B_o = 4,600G$. The distribution along the magnet axis (OY-axis) corresponds to the distribution in Figure 10. A decrease in the effective magnet length

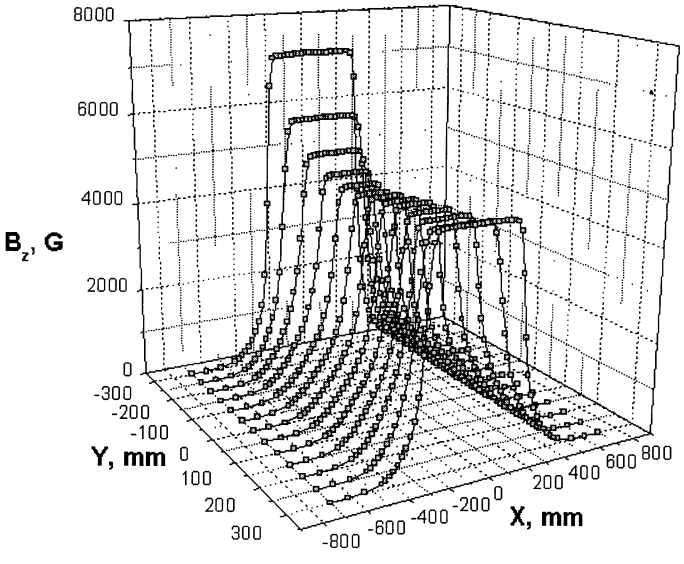

Fig.15. The measured distribution of the B_z-component of the magnetic field in the median plane of magnet M_3 at the field level $B_o = 4,600G$.

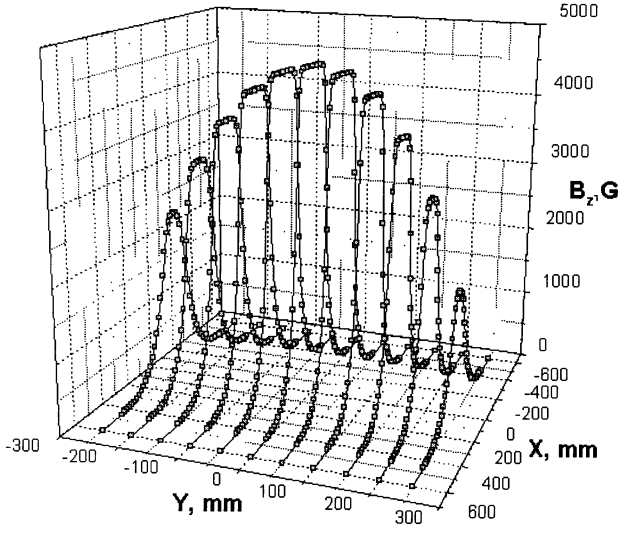

Fig.16. The measured distribution of the B_z-component of the magnetic field in the median plane of magnet M_4 at the field level $B_o = 4,600G$.

occurs in the region of the optical axis. The effective magnetic lengths behave in accordance with the concave shape of pole lateral faces. Similar measurements were performed for magnets M_4 (M_5). Figure 16 shows the magnetic field distribution in the median plane of magnet M_4. The distribution along the magnet axis (OY-axis) corresponds to the distribution in Figure 11. Notice that the field distribution corresponds to the convex shapes of the pole lateral faces.

Based on the calculations, the shimming of the pole pieces of magnets M_3, M_6 was made. The shims, mounted at radii of $-250, -200, -150, 0$, and $+250mm$ in M_3, M_6, compensated the lack of the field in the range of interest and, according to newly performed magnetic measurements, reduced the field deviations to a level of 1% for all the three field levels. The deviation in the effective magnetic lengths was reduced to less than 1% at the $B_o = 11,600G$ field level. The errors in the slope angle of effective magnetic borders were reduced to less than 0.5^o, 0.2^o, and 0.1^o for the field levels $B_o = 4,600, 11,600$, and $15,000G$, respectively. The additional correcting coils of pole surfaces of magnets M_4, M_5 should be used to compensate for the deviations. The use of the correcting coils will permit one to decrease the error to less than 0.2^o for all the field levels.

7.6 Magnetic field distributions in the non-median planes

One of the main purposes of the three-component magnetic field measurements was to obtain 3D- magnetic field maps for all the magnets for subsequent computerized particle raytracing through the entire separator.

For this purpose, the B_x , B_y , and B_z field components in magnets M_1 (M_8) were measured in 15 planes - in the median plane and in parallel planes situated below and above the median plane. Planes were spaced with a step of $10mm$ in the range from $\pm 70mm$ at a maximum gap size to $\pm 25mm$ at a minimum gap size.

Figures 17 and 18 represent, respectively, the B_x and B_y field components of magnet M_1 measured in the plane situated $30mm$ below the median plane at the field level $B_o = 7,050G$. The B_x field component is the projection of the magnetic field vector on an unit vector tangential to the optical axis of magnet M_1 located at the centre of the magnet. The component B_y is the projection of B on the direction along the bending radius pointing towards larger radii.

Figure 19 presents the measured distribution of the component B_z in the plane situated $30mm$ below the median plane at the field level $B_o = 7,050G$. The character of the distribution in the central section repeats that for the median plane (see Figure 9). As compared with the behaviour of B_z in the median plane (see Figure 13), the values of B_z in this distribution drop faster from their maximum values to zero as the effective field boundaries are crossed.

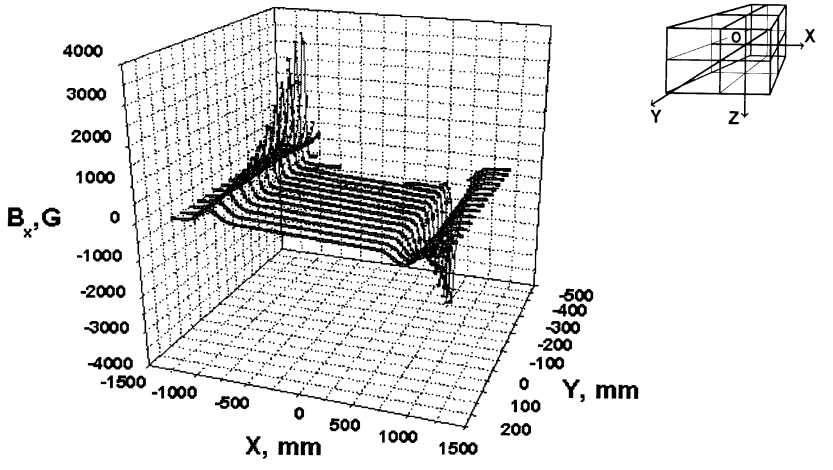

Fig.17. The measured distribution of the B_x-component of the magnetic field in the plane $30mm$ below the median plane of magnet M_1 at the field level $B_o = 7,050G$.

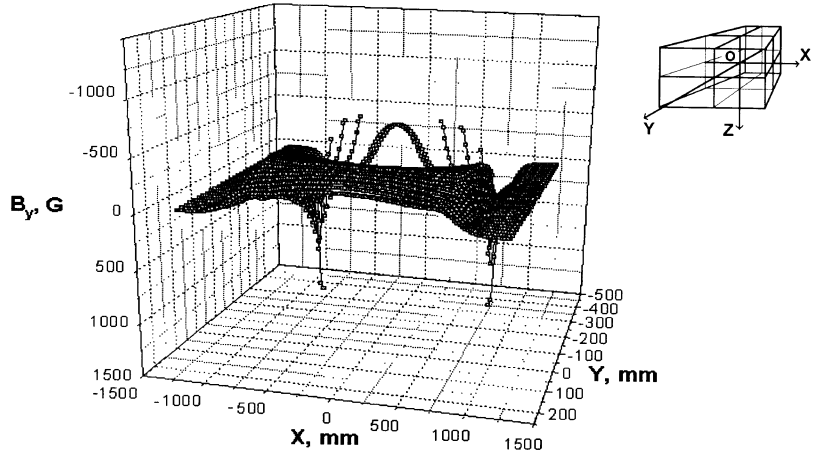

Fig.18. The measured distribution of the B_y-component of the magnetic field in the plane $30mm$ below the median plane of magnet M_1 at the field level $B_o = 7,050G$.

The B_φ, B_y , and B_z field components in magnets $M_2(M_7)$ were also measured on the closed surface described above (see section 7.3). The measurements of the B_φ and B_z field components near the lower pole piece are presented. Figure 20 shows the B_φ field component measured in 5 planes situated close to the lower pole of magnet M_2 at distances of $-45, -40, -35, -30$, and $-25mm$ from the median plane

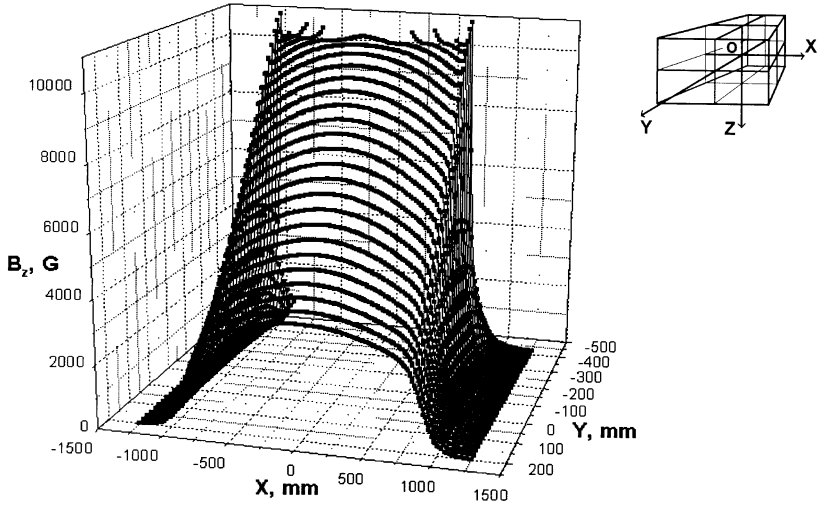

Fig.19. The measured distribution of the B_z-component of the magnetic field in the plane $30mm$ below the median plane of magnet M_1 at the field level $B_o = 7,050G$.

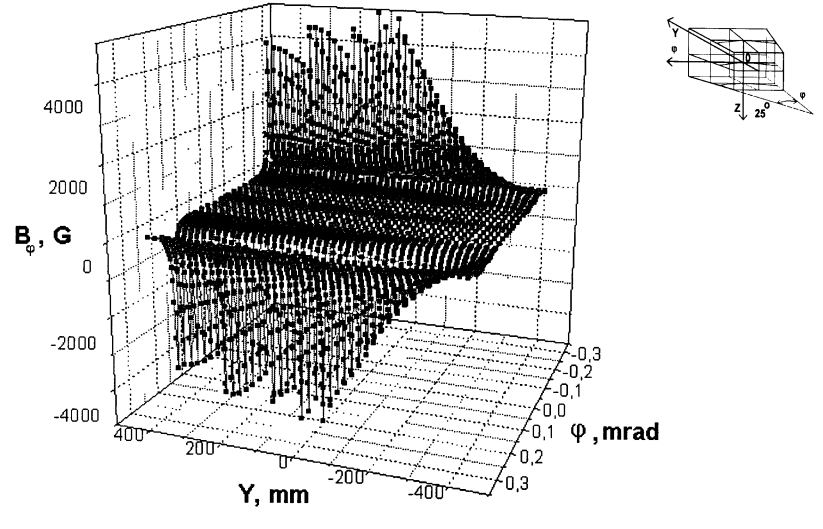

Fig.20. The measured distribution of the B_φ-component of the magnetic field close to the lower pole of magnet M_2 at distances $-45, -40, -35, -30$, and $-25mm$ from the median plane at the field level of $B_o = 11,600G$.

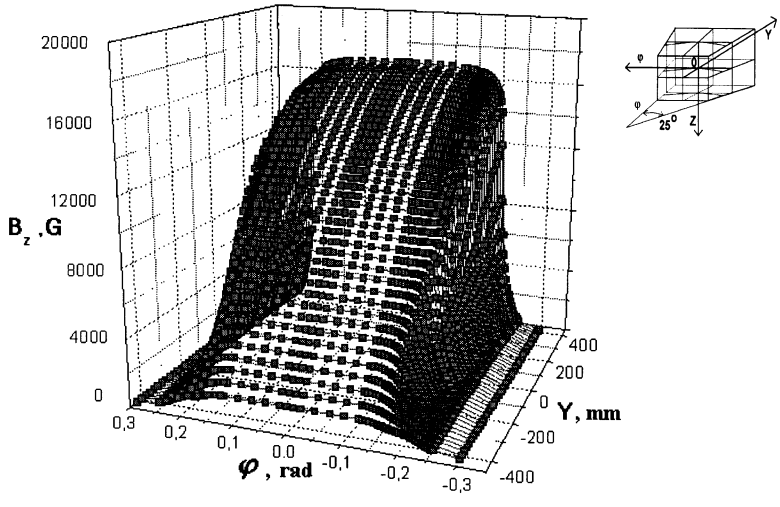

Fig.21. The measured distribution of the B_z-component of the magnetic field close to the lower pole of magnet M_2 at distances $-45, -40, -35, -30$, and $-25mm$ from the median plane at the field level of $B_o = 11,600G$.

at the field level $B_o = 11,600G$. The B_φ field component is the projection of the magnetic field vector on a unit vector tangential to the optical axis of magnet M_2. The absolute values of the B_φ maximum (minimum) near the entrance (exit) EFBs are bigger at bigger Y values. This is due to smaller gap sizes and, hence, higher magnetic flux densities in the region of larger Y values. Sharp jumps of the field values in the B_φ distribution are due to the fact that the component was measured in 5 different planes situated at different distances from the median plane.

Figure 21 presents the measured distribution of the component B_z in planes near the lower pole of magnet M_2 for the field level $B_o = 11,600G$. The distribution in the central section repeats that for the median plane (see Figure 10). As compared with the B_z behaviour in the median plane (see Figure 14), the values of B_z drop faster from its maximum values to zero near the lower pole when the effective field boundaries are crossed.

8 Main results and future developments

The performed magnetic field measurements showed the satisfactory performance of the separator magnets. Saturation effects are noticeable at high values of the magnetic field in the narrow gap. In the vicinity of the optical axis this

brings some optical parameters of the magnets closer to their design values (for pairs $M_1(M_8)$, $M_2(M_7)$, and $M_3(M_6)$), but, on the other hand, narrows working pole widths (in $M_1(M_8)$ and $M_2(M_7)$). After the field distribution analysis, we decided not to treat further the pole pieces of magnets $M_1(M_8)$ and $M_2(M_7)$. For magnets $M_3(M_6)$ and $M_4(M_5)$, the field distribution analysis and relevant trajectory simulations based on the results of measurements gave their realistic working pole widths. These data were used for shimming magnets $M_3(M_6)$. For magnets $M_4(M_5)$, correcting coils were manufactured and mounted on the pole pieces. Distribution errors of less than 1% for magnets $M_1(M_8)$, $M_3(M_6)$ and $M_4(M_5)$ and 2% for magnets $M_2(M_7)$ did not cause essential distortions of optical properties of the separator design. Raytracing simulations and the first experiments on spectra measurements for energetic heavy ion products showed that the main separator characteristics meet, in general, the design values.

The measured magnetic field distributions will be used for trajectory simulations. Further improvement of the separator parameters will be achieved by using the pole surface correcting coils of magnets $M_4(M_5)$.

To generate a 3D- field map for the trajectory analysis, it seems advisable to carry out advanced calculations for the actual M_1-M_8 design by using refined data on steel nonlinearity, shimming, the magnetic properties of the vacuum vessel, the geometry of coils, etc. This is of prime importance for magnets M_3-M_6 with essentially spatial fields. A special procedure has been developed for reconstruction the field within a closed volume from boundary measurements (12). The procedure is based on the modified finite-element code KOMPOT and the widely accepted approach of solving a boundary problem for estimation of the field (13). Numerical experiments revealed that a measurement error tends to decrease with a shift from the boundary. Using the measured data and simulation results, we are planning to construct a real three-dimensional field map of the separator.

Acknowledgments

The authors are indebted to V.K.Makoveev and V.S.Shvetsov for their assistance in the magnetic measurements of magnets $M_1(M_8)$ and $M_2(M_7)$, and to A.V.Nikiforovski and A.V.Bushuev for their assistance in the magnetic measurements of magnets $M_1(M_8)$.

This work is supported by grants INTAS-93-496 and RFBR-96-02-17214.

References

[1] A.G.Artukh et al., Nucl. Instr. and Meth. A 306 (1991) 123; A.G.Artukh et al., Nucl. Instr. and Meth. A 426 (1999) 605.

[2] A.G.Artukh et al., Sci. Rep. 1995-1996 FLNR JINR, E7-97-206, Dubna, 1997, p.250, 252, 254, 256, 258, 260, 262.

[3] S.M.Ananjev et al., Wide aperture magnets of the spectrometer COMBAS.- Dubna, 1993, Proc. XIII Conference on charge particle accelerators.V.1, p.314-319.

[4] M.G.Nagaenko, BETRAMF - a computer program for calculation and optimization of magneto-optical systems in linear approximation. - Leningrad, 1983, 26p., (Preprint NIIEFA:B-0614).

[5] M.G.Nagaenko, TOREX - a program for calculation of aberration coefficients of magneto-optical system. - M., CNNI Atominform, 1984, 15p., (Preprint NIIEFA:P-E-0655).

[6] M.G.Nagaenko, A complex of programs for calculation of beam transport systems and forming of beams of charge particles, in: Proc. Int. Conference on mathematical simulation, programming and mathematical methods of physics problems solving (Dubna, September 20-23,1983) - Dubna, JINR (D-10,11-84-818), 1985,p.264.

[7] K.L.Brown, Report Submitted to the 3rd Int. Magnet Symposium Held in Hamburg, Germany-May 1970. In: TRANSPORT Appendix, TRANSPORT Manual, Fermilab, December 1977, p.212.

[8] V.S.Kashikhin et al."Magneto-optical System of Large Acceptance Channel for Radioctive Nuclei Separation". In:proc. of the IEEE MT12 Conference, pp.564-567, 1992.

[9] V.S.Kashikhin, Programs SCALAR, VECTOR, FESS - numerical simulation of electromagnetic systems of electrophysical apparatus. - St.-Petersburg, 1983, 21p., (Preprint NIIEFA: B-0598).

[10] N.I.Doinikov, E.A.Lamsin, S.E.Sytchevsky, On computation of 3D magnetostatic fields of electrophysical apparatus magnet systems. - IEEE Trans. On Magn V.28, No 1, Jan.1999, pp.908-911.

[11] M.Berz, COSY INFINITY, Version 7, User's Guide and Reference Manual, Michigan State University, 1996.

[12] D.Baranov et al., An efficient algorithm of the reconstruction of spatial field with the use of the date determinate at the region boundary. In proc.: 5 EPAC 96 Conf., Sitges (Barselona) 1996, V.3, pp.1262-1264.

[13] H.Wind, Evaluating a magnetic field component from boundary of the observation only, Nucl. Instr. and Meth. V.84, N1, 1970, pp.117-128.

Received by Publishing Department
on October 13, 2000.

Артюх А.Г. и др. E13-2000-243
Широкоапертурные мультипольные магниты сепаратора КОМБАС

В Лаборатории ядерных реакций им. Г.Н.Флерова ОИЯИ создан и введен в эксплуатацию высокоразрешающий широкоапертурный сепаратор КОМБАС. Его магнитооптическая структура основана на принципе жесткой фокусировки. Поля анализирующих магнитов M_1, M_2, M_7 и M_8 содержат квадрупольные компоненты чередующегося знака, что позволяет обеспечить заданную фокусировку пучка. Кроме того, поля всех магнитов M_1 – M_8 содержат секступольную и октупольную компоненты магнитного поля, которые минимизируют аберрации 2-го и 3-го порядков. Все это позволило увеличить апертуру магнитов, эффективно сформировать пучок нужного размера и сократить длину канала. Такое использование широкоапертурных магнитов с комбинированными функциями является уникальным в технике изготовления сепараторов. Были выполнены трехкомпонентные магнитные измерения полей магнитов. Измеренные данные позволят реконструировать трехмерные карты полей всех магнитов. Трехмерные карты полей предполагается использовать для выполнения расчетов по трассировке частиц через сепаратор.

Работа выполнена в Лаборатории ядерных реакций им. Г.Н.Флерова ОИЯИ.

Препринт Объединенного института ядерных исследований. Дубна, 2000

Artukh A.G. et al. E13-2000-243
Wide Aperture Multipole Magnets of Separator COMBAS

The high-resolving wide aperture separator COMBAS has been designed and commissioned at the FLNR, JINR. Its magneto-optical structure is based on strong focusing principle. The magnetic fields of analysing magnets M_1, M_2, M_7, M_8, contain quadrupole components of alternating sign that provide necessary beam focusing. Besides, all the magnets M_1 – M_8, contain sextupole and octupole field components, which minimizes the 2nd and 3rd order aberrations. All this allowed one to increase their apertures, to effectively form a beam of the required sizes, and to decrease the channel length. This implementation of wide aperture magnets with combined functions is unique for the separation technology. Three-components magnetic measurements of all the magnets were performed. The measured data allow reconstructing the 3D-distributions of the fields in all the magnets. 3D-maps are supposed to be used for particle trajectory simulations throughout the entire separator.

The investigation has been performed at the Flerov Laboratory of Nuclear Reactions, JINR.

Preprint of the Joint Institute for Nuclear Research. Dubna, 2000

Макет Т.Е.Попеко

Подписано в печать 30.10.2000
Формат 60 × 90/16. Офсетная печать. Уч.-изд. листов 3,15
Тираж 335. Заказ 52309. Цена 3 р. 80 к.

Издательский отдел Объединенного института ядерных исследований
Дубна Московской области